Mixed Methods Using Standard Conforming Finite Elements

Jichun Li[1], Todd Arbogast[2], and Yunqing Huang[3]

[1]Department of Mathematical Sciences, University of Nevada,
Las Vegas, Nevada, U.S.A.
[2]Institute for Computational Engineering & Sciences, University of Texas, Austin,
Texas, U.S.A. Supported by National Science Foundation grant DMS-0713815.
[3]Hunan Key Laboratory for Computation and Simulation in Science
and Engineering, Xiangtan University, P.R.China.
Supported by the NSFC for Distinguished Young Scholars (10625106)
and National Basic Research Program of China under the grant 2005CB321701.

June 26, 2008

Abstract. We investigate the mixed finite element method (MFEM) for solving a second order elliptic problem with a lowest order term, as might arise in the simulation of single phase flow in porous media. We find that traditional mixed finite element spaces are not necessary when a positive lowest order (i.e., reaction) term is present. Hence we propose to use standard conforming finite elements $Q_k \times (Q_k)^d$ on rectangles or $P_k \times (P_k)^d$ on simplices to solve for both the pressure and velocity field in d dimensions. The price we pay is that we have only sub-optimal order error estimates. With a delicate superconvergence analysis, we find some improvement for the simplest pair $Q_k \times (Q_k)^d$ with any $k \geq 1$, or for $P_1 \times (P_1)^d$, when the mesh is uniform and the solution has one extra order of regularity. We also prove similar results for both parabolic and second order hyperbolic problems. Numerical results using $Q_1 \times (Q_1)^2$ and $P_1 \times (P_1)^2$ are presented in support of our analysis. These observations allow us to simplify the implementation of the MFEM, especially for higher order approximations, as might arise in an *hp*-adaptive procedure.

Mathematics Subject Classification (2000): 65N30.

Keywords. Mixed finite element, elliptic, parabolic, hyperbolic, inf-sup condition.

1 Introduction

The mixed finite element method (MFEM) is often used to obtain approximate solutions to more than one unknown at the same time. For example, the MFEM is used to solve the problem of single-phase flow in porous media, described by a second order elliptic equation written as a system of two first order equations, to obtain approximations to both the pressure and Darcy velocity field simultaneously. As another example, Maxwell's equations are often solved to obtain both the magnetic and electric fields. Accordingly, we need a different finite element space for each unknown. Convergence is guaranteed if these two spaces are interrelated in that they satisfy the so-called discrete inf-sup condition, i.e., the Ladyzhenskaya-Babuška-Brezzi (LBB) condition [7, 25, 27].

The inf-sup condition complicates the definition of the finite element spaces. For example, in solving the single-phase flow problem, many complicated mixed finite element spaces have been proposed such as those of Raviart-Thomas-Nedelec [26, 24], Brezzi-Douglas-Marini [5], Brezzi-Douglas-Duràn-Fortin [6], Chen-Douglas [12], Brezzi-Fortin-Marini [8], and Arbogast-Wheeler [3]. More details can be consulted the books by Brezzi-Fortin [7] and Roberts-Thomas [27] and references therein. Due to the complicated nature of these mixed spaces, usually only the lowest order spaces are used in practical computations. Furthermore, some postprocessing is needed to visualize the numerical solution, since the degrees of freedom for the MFEM are not nodal based. Such postprocessing further complicates the implementation of the MFEM. Hence, it would be desirable in some cases to be able to use standard nodal basis finite element spaces in the MFEM. Such efforts have been carried out in the engineering community (e.g., [17, 29]).

In this paper, we approximate a second order elliptic equation, written in mixed form, by applying the standard conforming finite element spaces, $Q_k \times (Q_k)^d$ on rectangles or $P_k \times (P_k)^d$ on simplices in dimension $d = 2, 3$, where Q_k and P_k are continuous piecewise polynomials of degree k in each Cartesian variable separately for Q_k, and of total degree k for P_k. A careful investigation shows that these spaces can be successfully used to solve for both the pressure and velocity field when a reaction term is present, i.e., when a uniformly positive zeroth order term appears in the equation. Because the inf-sup condition is violated, however, we have suboptimal convergence properties, losing a single power of the mesh spacing h. On simplicial meshes, these spaces are smaller in their number of degrees of freedom than the Raviart-Thomas spaces for similar accuracy. In the rectangular mesh case, again for similar accuracy, these spaces are slightly larger than the Raviart-Thomas spaces. However our proposed spaces are much simpler to implement, especially when higher order spaces are desired, or when an *hp*-adaptive refinement procedure is implemented.

A locally conservative variant is easy to define, in which the scalar variable is approximated by a discontinuous space of Q_k or P_k piecewise polynomials. In fact, we can use P_k on both rectangular and simplicial meshes.

The convergence result is suboptimal, however, we can recover one-half power of h on uniform grids for $Q_k \times (Q_k)^d$ with any $k \geq 1$, or for $P_1 \times (P_1)^d$. Moreover, we recover a full power of h, and thereby obtain optimal accuracy, when the problem has periodic boundary conditions, as might arise, e.g., from a cell problem in homogenization. This analysis is based on Lin's integral identity technique developed in the early 1990's (see, e.g., [20, 23, 21, 33]) for proving general finite element method superconvergence. More details and applications of this technique can be found in the superconvergence books [9, 22].

Finally, we extend our results to parabolic and second order hyperbolic problems. To the best of our knowledge, no previous reference has pointed out the interesting properties we note in this paper for the standard spaces in a mixed context when a time derivative or uniformly positive zeroth order term appears. Because of their simplicity and convergence properties, they seem to be competitive with, and perhaps the better choice than, corresponding Raviart-Thomas spaces when (1) simplicial meshes are used, (2) problems with periodic boundary conditions are approximated with uniform rectangular grids, (3) higher order approximations are desired, and (4) when an *hp*-adaptive refinement procedure is implemented.

The rest of the paper is organized as follows. In Section 2, we formulate the MFEM for the elliptic single-phase flow problem using $Q_k \times (Q_k)^d$ and $P_k \times (P_k)^d$ spaces. Existence and uniqueness of the system is proved, and error estimates are obtained. We pay special attention to the size of our mixed spaces, and compare to some which satisfy the inf-sup condition. Our improved error

analysis is also presented here. In Sections 3 and 4, we generalize the results to parabolic and hyperbolic problems, respectively. In Section 5, we provide some numerical examples to illustrate our method and confirm our theoretical analysis. Section 6 concludes the paper.

2 The Elliptic Problem

Let $\Omega \subset \boldsymbol{R}^d$, $d = 2, 3$, be an open Lipschitz polygon or polyhedron. For simplicity, we consider the single-phase flow problem

$$-\nabla \cdot [D(\boldsymbol{x})\,(\nabla p - \boldsymbol{g}(\boldsymbol{x}))] + \alpha(\boldsymbol{x})\,p(\boldsymbol{x}) = f(\boldsymbol{x}) \quad \text{in } \Omega, \tag{1}$$

$$p = 0 \qquad \text{on } \partial\Omega, \tag{2}$$

where the reaction coefficient $\alpha(\boldsymbol{x}) \geq \alpha_{\min} > 0$ and $D(x) \geq D_{\min} > 0$. (Other boundary conditions, including nonhomogeneous Dirichlet and Neumann ones, could be treated by the techniques used in this paper, but we have restricted ourselves to the homogeneous Dirichlet condition for expository purposes.) Introduce $\boldsymbol{u} = -D(\nabla p - \boldsymbol{g})$ and transform (1)–(2) to the standard mixed form: Find $p \in L^2(\Omega)$ and $\boldsymbol{u} \in H(\mathrm{div}; \Omega)$ such that

$$(\alpha p, w) + (\nabla \cdot \boldsymbol{u}, w) = (f, w) \quad \forall\ w \in L^2(\Omega), \tag{3}$$

$$-(p, \nabla \cdot \boldsymbol{v}) + (\beta \boldsymbol{u}, \boldsymbol{v}) = (\boldsymbol{g}, \boldsymbol{v}) \quad \forall\ \boldsymbol{v} \in H(\mathrm{div}; \Omega), \tag{4}$$

where $\beta = D^{-1}$ and $(\cdot, \cdot)_\omega$ denotes the $L^2(\Omega)$ inner-product (we omit ω if $\omega = \Omega$).

2.1 Discretization.

Let T_h be a conforming quasiuniform finite element partition of Ω by either rectangular or simplicial elements of maximal diameter h. We propose the mixed finite element approximation: Find $p_h \in W^k_{h,0}$ and $\boldsymbol{u}_h \in \boldsymbol{V}^k_h$ such that

$$(\alpha p_h, w_h) + (\nabla \cdot \boldsymbol{u}_h, w_h) = (f, w_h) \quad \forall\ w_h \in W^k_{h,0}, \tag{5}$$

$$-(p_h, \nabla \cdot \boldsymbol{v}_h) + (\beta \boldsymbol{u}_h, \boldsymbol{v}_h) = (\boldsymbol{g}, \boldsymbol{v}_h) \quad \forall\ \boldsymbol{v}_h \in \boldsymbol{V}^k_h, \tag{6}$$

where, for $k \geq 1$, the mixed finite element spaces are $W^k_{h,0} = W^k_h \cap H^1_0(\Omega)$, and

$$W^k_h = \{w \in C^0(\Omega) : w|_R \in W^k_h(E), \forall E \in T_h\}, \tag{7}$$

$$\boldsymbol{V}^k_h = \{\boldsymbol{v} \in (C^0(\Omega))^d : \boldsymbol{v}|_E = (W^k_h(E))^d, \forall E \in T_h\}, \tag{8}$$

and where $W^k_h(E) = Q_k(E)$ or $P_k(E)$ for rectangular or simplicial elements, respectively. Note that our mixed spaces $\boldsymbol{V}^k_h$ are the simplest $(H^1(\Omega))^d$ elements, and not any of the standard mixed finite element spaces [7, 27].

If the standard nodal basis is used, we can interleave the pressure and velocity unknowns to obtain a linear system with a block-structured matrix. The matrix has the standard stencil in terms of its blocks, and each block is $(d+1) \times (d+1)$. If we separate the pressure and velocity unknowns, we obtain a more standard saddle point linear system. In any case, as with all mixed methods, we do not have a simple positive definite system, and some care must be exercised in solving the linear system. (In our numerical results below, we used a direct solver.)

Remark 2.1 *We note that we could have taken*

$$W_{h,0}^k = W_{h,0}^{D,k} = \{w : w|_R \in W_h^k(E), \forall E \in T_h,\ w = 0 \text{ on } \partial\Omega\};$$

that is, we could relax the continuity of the pressure approximating space. Moreover, in this case, we could replace $Q_k(E)$ by $P_k(E)$ on rectangles. Our suboptimal order error estimates below would continue to hold, but not our improved error estimates. However, this form of the method would satisfy the local mass conservation principle. That is, in this case, (5) *implies that on each element $E \in T_h$,*

$$(\alpha p_h, 1)_E + (\nabla \cdot \boldsymbol{u}_h, 1)_E = (\alpha p_h, 1)_E + (\boldsymbol{u}_h \cdot \boldsymbol{n}, 1)_{\partial E} = (f, 1)_E,$$

so that the net flux through ∂E, $(\boldsymbol{u}_h \cdot \boldsymbol{n}, 1)_{\partial E}$, is exactly related to the net external sources $(f, 1)_E$ and the reaction or accumulation $(\alpha p_h, 1)_E$ acting over E. This is an important property in certain applications (see, e.g., [14, 28, 1]*).*

Remark 2.2 *For Galerkin formulations, the Dirichlet boundary condition (BC) is essential and the Neumann BC is natural, whereas mixed methods have the opposite behavior. The Neumann boundary condition, being essential, is easily incorporated by fixing the normal components of $\boldsymbol{u}$ and $\boldsymbol{v}$ to the data and zero, respectively, and taking p in W_h^k. The Dirichlet BC is natural. For the nonhomogeneous case $p = p_D$ on $\partial\Omega$, we would modify* (4) *to read*

$$-(p, \nabla \cdot \boldsymbol{v}) + (\beta \boldsymbol{u}, \boldsymbol{v}) = (\boldsymbol{g}, \boldsymbol{v}) - (p_D, \boldsymbol{v} \cdot \boldsymbol{n}) \quad \forall\ \boldsymbol{v} \in H(div; \Omega),$$

and the method similarly. This BC is imposed naturally with both p_h and w_h in W_h^k. However, we have a larger finite element space (W_h^k versus $W_{h,0}^k$), and the BC is not set exactly. Therefore, we chose above to impose the Dirichlet BC as an essential BC. That is, we take p in W_h^k such that p agrees with p_D on $\partial\Omega$, and we restrict w_h to $W_{h,0}^k$.

2.2 Suboptimal order error estimates.

Let $\|\cdot\|_{k,\omega}$ denote the $H^k(\omega)$-norm, and let $|\cdot|_{k,\omega}$ be the $H^k(\omega)$-seminorm of highest derivatives only, wherein we omit ω if it is Ω. For function w, let w_I denote the standard Q_k or P_k interpolant. Then we have the well-known interpolation estimate

$$\|w_I - w\|_m \le Ch^{l+1-m}|w|_{l+1}, \quad \forall\ w \in H^s(\Omega),\ m = 0, 1,\ l = \min(k, s-1) \ge 1. \tag{9}$$

By quasiuniformity, we also have the inverse inequality

$$\|w_h\|_1 \le Ch^{-1}\|w\|_0, \quad \forall\ w \in W_h^k(\Omega). \tag{10}$$

Since (5)–(6) is a finite dimensional linear system, uniqueness implies existence, so consider $f = 0$ and $\boldsymbol{g} = \boldsymbol{0}$ in (5)–(6). Take $w_h = p_h$ and $\boldsymbol{v}_h = \boldsymbol{u}_h$, and then add the results to obtain

$$(\alpha p_h, p_h) + (\beta \boldsymbol{u}_h, \boldsymbol{u}_h) = 0,$$

from which uniqueness is seen.

Theorem 2.1 *Assume p and $\boldsymbol{u} = -D(\nabla p - \boldsymbol{g})$ lie in $H^{k+1}(\Omega)$. Let p_h and $\boldsymbol{u}_h$ be the solution of (5)–(6) with mixed spaces (7)–(8). Then one has the sub-optimal order error estimate*

$$||p - p_h||_0 + ||\boldsymbol{u} - \boldsymbol{u}_h||_0 \leq C\big\{|p|_{k+1} + |\boldsymbol{u}|_{k+1}\big\}h^k, \tag{11}$$

where $k \geq 1$ is the degree of the finite element spaces.

Proof. For any $w_h \in W_{h,0}^k$ and $\boldsymbol{v}_h \in \boldsymbol{V}_h^k$, subtracting (5)–(6) from (3)–(4) gives:

$$(\alpha(p_I - p_h), w_h) + (\nabla \cdot (\boldsymbol{u}_I - \boldsymbol{u}_h), w_h) = (\alpha(p_I - p), w_h) + (\nabla \cdot (\boldsymbol{u}_I - \boldsymbol{u}), w_h), \tag{12}$$

$$-(p_I - p_h, \nabla \cdot \boldsymbol{v}_h) + \big(\beta(\boldsymbol{u}_I - \boldsymbol{u}_h), \boldsymbol{v}_h\big) = \big(\beta(\boldsymbol{u}_I - \boldsymbol{u}), \boldsymbol{v}_h\big) - (p_I - p, \nabla \cdot \boldsymbol{v}_h). \tag{13}$$

Choosing $w_h = p_I - p_h$ and $\boldsymbol{v}_h = \boldsymbol{u}_I - \boldsymbol{u}_h$ in (12)–(13), respectively, and adding the results together, we obtain the estimate

$$\begin{aligned}
&\alpha_{\min}||p_I - p_h||_0^2 + \beta_{\min}||\boldsymbol{u}_I - \boldsymbol{u}_h||_0^2 \\
&\quad = (\alpha(p_I - p), p_I - p_h) + (\nabla \cdot (\boldsymbol{u}_I - \boldsymbol{u}), p_I - p_h) \\
&\qquad + \big(\beta(\boldsymbol{u}_I - \boldsymbol{u}), \boldsymbol{u}_I - \boldsymbol{u}_h\big) - (p_I - p, \nabla \cdot (\boldsymbol{u}_I - \boldsymbol{u}_h)) \\
&\quad \leq Ch^k\big\{[h|p|_{k+1} + |\boldsymbol{u}|_{k+1}]||p_I - p_h||_0 \\
&\qquad + h|\boldsymbol{u}|_{k+1}||\boldsymbol{u}_I - \boldsymbol{u}_h||_0 + h|p|_{k+1}||\nabla \cdot (\boldsymbol{u}_I - \boldsymbol{u}_h)||_0\big\},
\end{aligned} \tag{14}$$

where we used the interpolation estimate (9) in the last step. Using the Cauchy-Schwarz inequality, and the inverse estimate (10) to bound the divergence term, we have

$$||p_I - p_h||_0^2 + ||\boldsymbol{u}_I - \boldsymbol{u}_h||_0^2 \leq C\big\{|p|_{k+1} + |\boldsymbol{u}|_{k+1}\big\}h^{2k},$$

which along with the triangle inequality and the interpolation estimate (9) concludes our proof. ∎

From the simple proof above, we see that the usual discrete inf-sup condition for the mixed finite element method is *not* needed for elliptic problems with positive reaction terms. The price we pay is that we have only sub-optimal order error estimates and nonuniform convergence as $\alpha_{\min} \to 0$ (i.e., $C \to \infty$ in this limit).

When we choose standard mixed spaces satisfying the inf-sup condition, optimal order error estimates are obtained, and the bounding constant is independent of $\alpha_{\min}$. For example, consider Raviart-Thomas spaces [26] on a rectangular grid T_h. For $k \geq 1$, on a rectangle R,

$$\begin{aligned}
\tilde{W}_h^k &= \{w : w|_R \in Q_{k-1}(R), \forall R \in T_h\}, \\
\tilde{\boldsymbol{V}}_h^k &= \{\boldsymbol{v} \in H(\mathrm{div}; \Omega) : \boldsymbol{v}|_R \in Q_{k,k-1,\ldots,k-1}(R) \times \cdots \times Q_{k-1,\ldots,k-1,k}(R), \forall R \in T_h\},
\end{aligned}$$

where $Q_{k_1,\ldots,k_d}$ are polynomials of degree k_i in x_i for each $i = 1, ..., d$. The only continuity requirements are on the normal velocities across element boundaries. If p_I is the L^2-projection onto $\tilde{W}_h^k$, i.e.,

$$(p_I - p, w_h) = 0 \quad \forall\ w_h \in \tilde{W}_h^k, \tag{15}$$

and $\boldsymbol{u}_I$ as the Raviart-Thomas or Fortin projection operator for which

$$(\nabla \cdot (\boldsymbol{u}_I - \boldsymbol{u}), w_h) = 0 \quad \forall\ w_h \in \tilde{W}_h^k, \tag{16}$$

optimal order error estimate can be recovered immediately by using (15), (16), and the fact that $\nabla \cdot \boldsymbol{v}_h \subset \tilde{W}_h^k$ for any $\boldsymbol{v}_h \in \tilde{\boldsymbol{V}}_h^k$, since in this case the last terms in both (12) and (13) vanish. The independence on $\alpha_{\min}$ is more subtle, and follows from the uniformity of the inf-sup condition [7, 27].

2.3 Numbers of degrees of freedom.

We note that for accuracy of order $k \geq 1$, we have proposed using the continuous elements $Q_k \times (Q_k)^d$, which on an $N \times \cdots \times N$ grid of elements has dimension

$$\dim(W_{h,0}^k \times \boldsymbol{V}_h^k) = (kN-1)^d + d(kN+1)^d = O\big((d+1)k^d N^d\big).$$

Equivalent accuracy comes from using the Raviart-Thomas spaces [26, 24] $Q_{k-1} \times (Q_{k,k-1,\ldots,k-1} \times \cdots \times Q_{k-1,\ldots,k-1,k})$, which has dimension

$$\dim(\tilde{W}_h^{k-1} \times \tilde{\boldsymbol{V}}_h^{k-1}) = (kN)^d + d(kN+1)(kN)^{d-1} = O\big((d+1)k^d N^d\big),$$

which, although smaller, is not substantially so. The order of the number of degrees of freedom (DOFs), for large N, is the same for the two methods. In fact, when $d = 2$, the difference is exactly 3 for all k.

To be fair, however, the Raviart-Thomas spaces on (nonuniform) rectangular grids, at least in some cases, give superconvergence for both p and $\boldsymbol{u}$ [31, 2]. In such cases, we would need to compare to $Q_{k-2} \times (Q_{k-1,k-2,\ldots,k-2} \times \cdots \times Q_{k-2,\ldots,k-2,k-1})$, which has dimension

$$\dim(\tilde{W}_h^{k-2} \times \tilde{\boldsymbol{V}}_h^{k-2}) = (d+1)((k-1)N)^d + d((k-1)N)^{d-1} = O\big((d+1)(k-1)^d N^d\big),$$

which is smaller by a factor of $((k-1)/k)^d$. However, since the complexity of the Raviart-Thomas spaces is great, it may make sense to use the simpler standard spaces $W_{h,0}^k \times \boldsymbol{V}_h^k$, especially in an *hp*- or other adaptive procedure.

Furthermore, the Raviart-Thomas spaces give a locally conservative method. If this property is desired, we noted in Remark 2.1 that we would need to use $W_{h,0}^{D,k}$ for the scalar approximating space. Then the count would be somewhat larger. Using Q_k for the scalar would give

$$\dim(W_{h,0}^{D,Q,k} \times \boldsymbol{V}_h^k) = ((k+1)N-2)^d + d(kN+1)^d = O\big(((k+1)^d + dk^d)N^d\big),$$

but using P_k for the scalar would be the better choice, giving

$$\dim(W_{h,0}^{D,P,k} \times \boldsymbol{V}_h^k) \leq \binom{k+d}{d} N^d + d(kN+1)^d = O\left(\left(\frac{(k+d)!}{k!\,d!} + dk^d\right)N^d\right),$$

with the inequality due to the fact that we did not account for the Dirichlet boundary condition.

It is more difficult to compare simplicial meshes. For $d = 2$, consider a cross-hatched rectangular $N \times N$ grid (with $2N^2$ elements, as depicted in Figure 2 of Section 5). The continuous elements $P_k \times (P_k)^2$ give a space with dimension

$$\dim(W_{h,0}^k \times \boldsymbol{V}_h^k) = (kN-1)^2 + 2(kN+1)^2 = 3(kN)^2 + 2kN + 3 = O(3k^2N^2).$$

The locally conservative space has dimension

$$\begin{aligned}\dim(W_{h,0}^{D,k} \times \boldsymbol{V}_h^k) &= ((k+1)N-2)^2 + 2(kN+1)^2 \\ &= (3k^2+2k+1)N^2 - 4N + 6 = O\big((3k^2+2k+1)N^2\big).\end{aligned}$$

Equivalent accuracy comes from the Raviart-Thomas elements $P_{k-1} \times \big(\boldsymbol{x}P_{k-1} \oplus (P_{k-1})^2\big)$. The scalar space is fully discontinuous and has dimension

$$\dim \tilde{W}_h^{k-1} = \binom{k+1}{2} 2N^2 = k(k+1)N^2.$$

The vector variable space has normal continuity, so its dimension is $3\dim(P_{k-1})2N^2$ minus k times the number of internal edges; that is,

$$\dim \tilde{\boldsymbol{V}}_h^{k-1} = 6\binom{k+1}{2} N^2 - k\big(N^2 + 2N(N-1)\big) = 3(kN)^2 + 2kN.$$

Thus,

$$\dim(\tilde{W}_h^{k-1} \times \tilde{\boldsymbol{V}}_h^{k-1}) = (4k^2+k)N^2 + 2kN = O\big((4k^2+k)N^2\big),$$

which is larger than our proposed continuous spaces (assuming nontrivial $N \geq 2$), and larger than the locally conservative discontinuous spaces for $k > 1$.

Finally, consider $d = 3$ and a tetrahedral grid. Again, we restrict to a simple grid: a standard $N \times N \times N$ rectangular grid with either $n = 5$ or $n = 6$ tetrahedrons per grid cell. First we consider a single coordinate i of the vector variable space $\boldsymbol{V}_h^k$ using elements P_k. We count internal DOFs (if $k \geq 4$), then DOFs shared on faces (if $k \geq 3$), then DOFs shared on edges (if $k \geq 2$), and finally DOFs shared at vertices. This gives dimension

$$\begin{aligned}\frac{1}{3}\dim(\boldsymbol{V}_h^k) = \binom{k-1}{3} nN^3 + \binom{k-1}{2}\big(3(N+1)N^2 + (2n-6)N^3\big) \\ + (k-1)\big(3(N+1)^2N + (n-5)N^3\big) + (N+1)^3.\end{aligned}$$

The scalar space is similar:

$$\begin{aligned}\dim(W_{h,0}^k) = \binom{k-1}{3} nN^3 + \binom{k-1}{2}\big(3(N-1)N^2 + (2n-6)N^3\big) \\ + (k-1)\big(3(N-1)^2N + (n-5)N^3\big) + (N-1)^3.\end{aligned}$$

Thus,

$$\begin{aligned}\dim(W_{h,0}^k \times \boldsymbol{V}_h^k) &= 4\binom{k-1}{3} nN^3 + \binom{k-1}{2}\big(12N^3 + 6N^2 + 4(2n-6)N^3\big) \\ &\quad + (k-1)\big(12N(N^2+N+1) + 4(n-5)N^3\big) + 3(N+1)^3 + (N-1)^3 \\ &= \left(\frac{2n}{3}k^3 - 6k^2 + \left(10 - \frac{2n}{3}\right)k + 6\right)N^3 + 3k(k+1)N^2 + 12kN + 2.\end{aligned}$$

The discontinuous space count is similar, and results in

$$\begin{aligned}\dim(W_{h,0}^{D,k} \times \boldsymbol{V}_h^k) &\leq \binom{k+3}{3} nN^3 + \dim(\boldsymbol{V}_h^k) \\ &= \left(\frac{2n}{3}k^3 + \left(n - \frac{9}{2}\right)k^2 + \left(\frac{4n}{3} + \frac{15}{2}\right)k - n\right)N^3 + \frac{9}{2}k(k+1)N^2 + 9kN + 3.\end{aligned}$$

We compare this to the Raviart-Thomas space $P_{k-1} \times \big(\boldsymbol{x}P_{k-1} \oplus (P_{k-1})^3\big)$, for which

$$\begin{aligned}\dim(\tilde{W}_h^{k-1} \times \tilde{\boldsymbol{V}}_h^{k-1}) &= 5\binom{k+2}{3}nN^3 - \binom{k+1}{2}\big(6N^2(N-1) + (2n-6)N^3\big) \\ &= \left(\frac{5}{6}k^3 + \frac{3}{2}k^2 + \frac{2}{3}k\right)nN^3 + 3(k+1)kN^2,\end{aligned}$$

which is again larger than the proposed space for $k > 1$ and all nontrivial $N \geq 2$, and also now for $k = 1$ and $N \geq 4$ for $n = 5$ and $N \geq 3$ for $n = 6$.

2.4 Improved error estimates.

We can improve our error estimates if we use uniform C^0 rectangular elements. The key of the proof is to use Lin's integral identity superconvergence technique [22], encapsulated in the following lemma, in which we also state an extension of the results to the periodic case.

Lemma 2.1 *If T_h is a uniform rectangular partition, then there is $C > 0$, independent of h, such that, for any $w \in H^{k+2}(\Omega)$,*

$$\left|\left(\frac{\partial}{\partial x_i}(w_I - w), v_h\right)\right| \leq Ch^{k+1}||w||_{k+2}||v_h||_0, \quad \forall v_h \in W_{h,0}^k,\ i = 1, ..., d, \tag{17}$$

where $W_{h,0}^k$ contains continuous Q_k elements. Moreover, the result holds for all $v_h \in W_h^k$ provided that w is periodic.

The proof of (17) in Lin and Yan's book [22] is given in Chinese and rather sketchy in its details. Considering the elegance of the proof, our extension to the periodic case, its importance for our numerical examples later, and for completeness, we provide a detailed proof for the case $k = 1$ in the Appendix, Section 7). The proof for higher-order elements is similar, though very technical.

Returning to (14), we see that we can estimate, since $p_I - p_h \in W_{h,0}^k$,

$$|\nabla \cdot (\boldsymbol{u}_I - \boldsymbol{u}), p_I - p_h)| \leq Ch^{k+1}||\boldsymbol{u}||_{k+2}||p_I - p_h||_0. \tag{18}$$

The other divergence term in (14), $(p_I - p, \nabla \cdot (\boldsymbol{u}_I - \boldsymbol{u}_h))$, is more delicate, since $\boldsymbol{u}_I - \boldsymbol{u}_h \notin (W_{h,0}^k)^d$. For $\boldsymbol{v}_h \in \boldsymbol{V}_h^k$, let $\boldsymbol{v}_{h,0} \in (W_{h,0}^k)^d$ agree with $\boldsymbol{v}_h$ at degrees of freedom strictly inside Ω. The well known result

$$\|\boldsymbol{v}_h - \boldsymbol{v}_{h,0}\|_0 \leq Ch^{1/2}\|\boldsymbol{v}_h\|_0$$

combined with integration by parts and (17), enables us to obtain, for all $\boldsymbol{v}_h \in \boldsymbol{V}_h^k$,

$$\begin{aligned}|(p_I - p, \nabla \cdot \boldsymbol{v}_h)| &= |-(\nabla(p_I - p), \boldsymbol{v}_h)| \\ &\leq |-(\nabla(p_I - p), \boldsymbol{v}_{h,0})| + |-(\nabla(p_I - p), \boldsymbol{v}_h - \boldsymbol{v}_{h,0})| \\ &\leq Ch^{k+1/2}||p||_{k+2}||\boldsymbol{v}_h||_0.\end{aligned} \tag{19}$$

Substituting (18) and (19) into (14) and following the same proof for Theorem 2.1, we have the following error estimate, improved by a factor of $h^{1/2}$. The price we pay is that we need one extra order of regularity for the solution.

Theorem 2.2 *Assume $p, \boldsymbol{u} = -\nabla p + \boldsymbol{g} \in H^{k+1}(\Omega)$. Let p_h and $\boldsymbol{u}_h$ be the solution of* (5)–(6) *with mixed spaces* (7)–(8) *on rectangles. If T_h is a uniform rectangular partition, then*

$$||p - p_h||_0 + ||\boldsymbol{u} - \boldsymbol{u}_h||_0 \leq C\big\{|p|_{k+2} + |\boldsymbol{u}|_{k+2}\big\}h^{k+1/2}, \tag{20}$$

where $k \geq 1$ is the degree of the finite element spaces. Moreover, if p is periodic, the estimate holds optimally, i.e., with $h^{k+1/2}$ replaced by h^{k+1}.

Theorem 2.3 *The estimate* (17) *holds for P_1 elements on uniform conforming triangular meshes (i.e., uniform in three directions). Hence, in this case, the following improved error estimate holds:*

$$||p - p_h||_0 + ||\boldsymbol{u} - \boldsymbol{u}_h||_0 \leq C\big\{|p|_3 + |\boldsymbol{u}|_3\big\}h^{3/2}. \tag{21}$$

Proof. We need only prove (17). We assume that T_h is a uniform triangulation of Ω; that is, there are directions $\vec{l}_1, \vec{l}_2, \vec{l}_3$ such that any edge is parallel to one of those directions (see, e.g., Figure 2 of Section 5). Let D_i be the directional derivative along $\vec{l}_i$, i.e., $D_i = \vec{l}_i \cdot \nabla$, and recall that

$$W_h^1(\Omega) = \{v \in H^1(\Omega) : v|_\tau \text{ is linear } \forall\ \tau \in T_h\}.$$

For any $v \in W_h^1(\Omega)$, we have [32, p. 1017–1018]

$$(w - w_I, v_x) = \sum_{\tau \in T_h} \int_\tau (w - w_I)v_x = -\frac{h^2}{24} \sum_{\tau \in T_h} \int_\tau \sum_{i=1}^3 \lambda_i^2 D_i^2 w \cdot v_x + O(h^2)||w||_3||v||_0,$$

where λ_i are some constants independent of h, depending only on the relative lengths of the triangle edges. Thus, for $v \in W_{h,0}^1$,

$$\begin{aligned}
((w_I - w)_x, v) &= (w - w_I, v_x) \\
&= -\frac{h^2}{24} \sum_{\tau \in T_h} \int_\tau \sum_{i=1}^3 \lambda_i^2 D_i^2 w \cdot v_x + O(h^2)||w||_3||v||_0 \\
&= \frac{h^2}{24} \int_\Omega \sum_{i=1}^3 \lambda_i^2 (D_i^2 w)_x \cdot v - \frac{h^2}{24} \int_{\partial\Omega} \sum_{i=1}^3 \lambda_i^2 D_i^2 w \cdot v\, n_x + O(h^2)||w||_3||v||_0 \\
&= O(h^2)||w||_3||v||_0,
\end{aligned}$$

where $\vec{n} = (n_x, n_y)$ is the unit outward normal. Note that in the last step we used the fact that integration along interior element edges cancel due to the mesh uniformity. Furthermore, since $v \in W_{h,0}^1$, then the boundary integral term vanishes also. Hence we have obtained the result (17) for x-derivatives. A similar argument gives the result for the y-derivative. □

3 The Parabolic Problem

In this section, we show that similar results as above hold for the parabolic problem. For simplicity, we consider the parabolic equation

$$\alpha(\boldsymbol{x})p_t - \nabla \cdot [D(\boldsymbol{x})(\nabla p - \boldsymbol{g}(\boldsymbol{x}, t))] = f(\boldsymbol{x}, t) \quad \text{in } \Omega \times (0, T), \tag{22}$$

$$p = 0 \quad \text{on } \partial\Omega \times (0, T), \tag{23}$$

$$p(\boldsymbol{x}, 0) = p_0(\boldsymbol{x}) \quad \text{on } \Omega. \tag{24}$$

If $\Omega \subset R^d$ $(d = 2, 3)$ is a bounded domain with $\partial\Omega \in C^2$, and

$$D_{ij}(\boldsymbol{x}) \in C^{0,1}(\overline{\Omega}),\ \alpha(\boldsymbol{x}) \in L^\infty,\ f, \nabla\cdot\boldsymbol{g} \in L^2(Q),\ p_0 \in H_0^1(\Omega),$$
$$D_{ij}\xi_i\xi_j \geq \gamma|\xi|^2,\ \forall\ \boldsymbol{x} \in \Omega,\ \xi \in R^d,$$

then there exists [15, 30] a unique solution $p \in L^2(0,T;H^2(\Omega)) \cap H^1(0,T;L^2(\Omega))$ to (22)-(24). Introduce $\boldsymbol{u} = -D(\nabla p + \boldsymbol{g})$ and transform (22)–(23) to the standard mixed form (wherein $\beta = D^{-1}$): For any $t \in (0,T)$, find $p(t) \in L^2(\Omega)$ and $\boldsymbol{u}(t) \in H(\mathrm{div};\Omega)$ such that

$$(\alpha p_t, w) + (\nabla\cdot\boldsymbol{u}, w) = (f, w) \quad \forall\ w \in L^2(\Omega), \tag{25}$$
$$(\beta\boldsymbol{u}, \boldsymbol{v}) - (p, \nabla\cdot\boldsymbol{v}) = (\boldsymbol{g}, \boldsymbol{v}) \quad \forall\ \boldsymbol{v} \in H(\mathrm{div};\Omega). \tag{26}$$

Lemma 3.1 *The following stability estimates hold:*

$$\text{(i)}\quad ||p||_{L^\infty(0,T;L^2(\Omega))} + ||\boldsymbol{u}||_{L^2(0,T;L^2(\Omega))} \leq C\{||f||_{L^2(0,T;L^2(\Omega))} + ||\boldsymbol{g}||_{L^2(0,T;L^2(\Omega))}\},$$
$$\text{(ii)}\quad ||p_t||_{L^2(0,T;L^2(\Omega))} + ||\boldsymbol{u}||_{L^\infty(0,T;L^2(\Omega))} \leq C\{||f||_{L^2(0,T;L^2(\Omega))} + ||\boldsymbol{g}_t||_{L^2(0,T;L^2(\Omega))}\},$$
$$\text{(iii)}\quad ||\nabla\cdot\boldsymbol{u}||_{L^2(0,T;L^2(\Omega))} \leq C\{||f||_{L^2(0,T;L^2(\Omega))} + ||\boldsymbol{g}_t||_{L^2(0,T;L^2(\Omega))}\}.$$

Above we used the Bochner space $L^r(T;X)$ with the corresponding norm defined as follows:

$$||u||_{L^r(T;X)} = \Big(\int_T ||u(t)||_X^r dt\Big)^{1/r} < \infty, \quad 1 \leq r < \infty,$$
$$||u||_{L^\infty(T;X)} = \operatorname*{ess\,sup}_{t\in T} ||u(t)||_X < \infty.$$

This result is well-known in the nonmixed context. We recast it in mixed form for our purposes, and provide a proof, since the techniques are used in the error analysis to follow.

Proof. (i) Taking $w = p$ and $\boldsymbol{v} = \boldsymbol{u}$ in (25) and (26), respectively, and adding together, we obtain

$$\frac{1}{2}\frac{d}{dt}||\sqrt{\alpha}p||_0^2 + ||\sqrt{\beta}\boldsymbol{u}||_0^2 = (f,p) + (\boldsymbol{g},\boldsymbol{u}) \leq ||\alpha^{-1/2}f||_0||\sqrt{\alpha}p||_0 + ||\beta^{-1/2}\boldsymbol{g}||_0||\sqrt{\beta}\boldsymbol{u}||_0,$$

which along with Gronwall's inequality concludes the proof.

(ii) Taking $w = p_t$ in (25), differentiating (26) with respect to t and taking $\boldsymbol{v} = \boldsymbol{u}$, and adding together, we obtain

$$||\sqrt{\alpha}p_t||_0^2 + \frac{1}{2}\frac{d}{dt}||\sqrt{\beta}\boldsymbol{u}||_0^2 = (f,p_t) + (\boldsymbol{g}_t,\boldsymbol{u}) \leq ||\alpha^{-1/2}f||_0||\sqrt{\alpha}p_t||_0 + ||\beta^{-1/2}\boldsymbol{g}_t||_0||\sqrt{\beta}\boldsymbol{u}||_0,$$

which along with Gronwall's inequality concludes the proof.

(iii) Taking $w = \nabla\cdot\boldsymbol{u}$ in (25), we obtain

$$||\nabla\cdot\boldsymbol{u}||_0^2 = (f, \nabla\cdot\boldsymbol{u}) - (\alpha p_t, \nabla\cdot\boldsymbol{u}) \leq \big(||f||_0 + ||\alpha p_t||_0\big)||\nabla\cdot\boldsymbol{u}||_0,$$

which along with (ii) concludes the proof. □

There are many existing works on mixed finite element methods for parabolic problems (e.g., [10, 19]), which are based on Raviart-Thomas spaces. We propose a semi-discrete mixed finite element approximation for (25)–(26): Find $p_h \in W_{h,0}^k$ and $\boldsymbol{u}_h \in \boldsymbol{V}_h^k$ such that

$$(\alpha p_{h,t}, w_h) + (\nabla\cdot\boldsymbol{u}_h, w_h) = (f, w_h) \quad \forall\ w_h \in W_{h,0}^k, \tag{27}$$
$$(\beta\boldsymbol{u}_h, \boldsymbol{v}_h) - (p_h, \nabla\cdot\boldsymbol{v}_h) = (\boldsymbol{g}, \boldsymbol{v}_h) \quad \forall\ \boldsymbol{v}_h \in \boldsymbol{V}_h^k, \tag{28}$$

with initial condition

$$p_h(\boldsymbol{x}, 0) = p_{0,I}(\boldsymbol{x}), \tag{29}$$

where $p_{0,I}$ denotes the standard Q_k or P_k interpolant of $p_0(\boldsymbol{x})$ into $W^k_{h,0}$. Here the mixed finite element spaces are the same as for the elliptic case (7)–(8) above.

Existence and uniqueness for (27)–(28) can be proved as follows. Working over a finite element vector space basis, we rewrite (27)–(28) as

$$AP_t + BU = F, \tag{30}$$

$$-B^T P + DU = G, \tag{31}$$

where A and D are symmetric positive definite matrices. Solving (31) for U and substituting into (30) gives us

$$AP_t + BD^{-1}B^T P = F - BD^{-1}G, \tag{32}$$

which has a unique solution, since it is a linear system of ordinary differential equations with a given initial condition $P(0)$. Hence, for any $t > 0$, (27)–(29) has a unique solution.

The three stability results of Lemma 3.1 hold true for our discrete solution $(p_h, \boldsymbol{u}_h)$.

Theorem 3.1 *Assume $p(\cdot,t)$, $p_t(\cdot,t)$, and $\boldsymbol{u}(\cdot,t) = -D(\nabla p(\cdot,t) - \boldsymbol{g}(\cdot,t))$ lie in $H^{k+1}(\Omega)$. Let p_h and u_h be the solution of* (27)–(28) *with mixed spaces* (7)–(8)*. Then there is a constant C such that the sub-optimal order error estimate*

$$||p - p_h||_{L^\infty(0,T;L^2(\Omega))} + ||\boldsymbol{u} - \boldsymbol{u}_h||_{L^2(0,T;L^2(\Omega))} \leq C\Big\{ \int_0^T \big(|p_t|^2_{k+1} + |p|^2_{k+1} + |\boldsymbol{u}|^2_{k+1}\big)\, dt \Big\}^{1/2} h^k \tag{33}$$

holds, where $k \geq 1$ is the degree of the finite element spaces.

Proof. For any $w_h \in W^k_{h,0}$ and $\boldsymbol{v}_h \in \boldsymbol{V}^k_h$, subtracting (27)–(28) from (25)–(26) yields

$$(\alpha(p_I - p_h)_t, w_h) + (\nabla \cdot (\boldsymbol{u}_I - \boldsymbol{u}_h), w_h) = (\alpha(p_I - p)_t, w_h) + (\nabla \cdot (\boldsymbol{u}_I - \boldsymbol{u}), w_h), \tag{34}$$

$$(\beta(\boldsymbol{u}_I - \boldsymbol{u}_h), \boldsymbol{v}_h) - (p_I - p_h, \nabla \cdot \boldsymbol{v}_h) = (\beta(\boldsymbol{u}_I - \boldsymbol{u}), \boldsymbol{v}_h) - (p_I - p, \nabla \cdot \boldsymbol{v}_h). \tag{35}$$

Choosing $w_h = p_I - p_h$ and $\boldsymbol{v}_h = \boldsymbol{u}_I - \boldsymbol{u}_h$ in (34)–(35) and adding the equations together, we obtain the estimate

$$\begin{aligned}
&\frac{1}{2}\frac{d}{dt}||\sqrt{\alpha}(p_I - p_h)||^2_0 + ||\sqrt{\beta}(\boldsymbol{u}_I - \boldsymbol{u}_h)||^2_0 \\
&\quad = (\alpha(p_I - p)_t, p_I - p_h) + (\nabla \cdot (\boldsymbol{u}_I - \boldsymbol{u}), p_I - p_h) \\
&\qquad + (\beta(\boldsymbol{u}_I - \boldsymbol{u}), \boldsymbol{u}_I - \boldsymbol{u}_h) - (p_I - p, \nabla \cdot (\boldsymbol{u}_I - \boldsymbol{u}_h)) \\
&\quad \leq Ch^k\big\{[h|p_t|_{k+1} + |\boldsymbol{u}|_{k+1}]||p_I - p_h||_0 \\
&\qquad + h|\boldsymbol{u}|_{k+1}||\boldsymbol{u}_I - \boldsymbol{u}_h||_0 + h|p|_{k+1}||\nabla \cdot (\boldsymbol{u}_I - \boldsymbol{u}_h)||_0\big\}.
\end{aligned} \tag{36}$$

Using the Cauchy-Schwarz inequality, the inverse estimate (10), and Gronwall's inequality, we have

$$||(p_I - p_h)(t)||^2_0 + \int_0^t ||\boldsymbol{u}_I - \boldsymbol{u}_h||^2_0\, dt \leq Ch^{2k},$$

which along with the triangle inequality and the interpolation estimate (9) concludes our proof. □

From our proof, it is obvious that the discrete inf-sup conditions can be avoided when solving parabolic problems by mixed methods (e.g., [11, 13, 18]). The price we pay is that we only have sub-optimal order error estimates. When we choose those well-known mixed spaces satisfying the inf-sup condition, it is easy to show that the optimal order error estimate can be recovered by following the exact proof as we did for the elliptic problem.

Remark 3.1 *Similar to the elliptic problem, improved error estimates can be recovered on uniform grids by using Lin's integral identity in Lemma* 2.1 [22]. *For rectangular elements* $Q_k \times (Q_k)^d$ *or triangular* $P_1 \times (P_1)^d$, *substituting* (17) *and* (19) *into* (36) *and following the same proof for Theorem* 3.1, *we have the improved error estimate*

$$||p - p_h||_{L^\infty(0,T;L^2(\Omega))} + ||\boldsymbol{u} - \boldsymbol{u}_h||_{L^2(0,T;L^2(\Omega))} \leq Ch^{k+1/2}. \tag{37}$$

The price we pay is that we need one extra order of regularity for the solution.

Remark 3.2 *Similar results hold true for fully (i.e., time) discrete approximations of* (25)–(26), *such as backward Euler or Crank-Nicolson time stepping procedures, provided that the time step is sufficiently small (as required by the discrete Gronwall inequality).*

4 The Hyperbolic Problem

We now turn to the hyperbolic problem, which for simplicity we take merely the wave equation

$$p_{tt} - \triangle p = f \qquad \text{in } \Omega \times (0,T) \tag{38}$$
$$p = 0 \qquad \text{on } \partial\Omega \times (0,T) \tag{39}$$
$$p(\boldsymbol{x},0) = p_0(\boldsymbol{x}), \quad \forall\ \boldsymbol{x} \in \Omega, \tag{40}$$
$$p_t(\boldsymbol{x},0) = p_1(\boldsymbol{x}), \quad \forall\ \boldsymbol{x} \in \Omega. \tag{41}$$

By introducing $\sigma = p_t$ and $\boldsymbol{u} = -\nabla p$, we obtain the mixed weak formulation: Find $\sigma(\cdot,t) \in L^2(\Omega)$ and $\boldsymbol{u}(\cdot,t) \in H(\mathrm{div};\Omega)$ such that

$$(\sigma_t, w) + (\nabla \cdot \boldsymbol{u}, w) = (f, w) \quad \forall\ w \in L^2(\Omega), \tag{42}$$
$$(\boldsymbol{u}_t, \boldsymbol{v}) - (\sigma, \nabla \cdot \boldsymbol{v}) = 0 \qquad \forall\ \boldsymbol{v} \in H(\mathrm{div};\Omega), \tag{43}$$

from which we can construct our mixed finite element method: Find $\sigma_h \in W_{h,0}^k$ and $\boldsymbol{u}_h \in \boldsymbol{V}_h^k$ such that

$$(\sigma_{h,t}, w_h) + (\nabla \cdot \boldsymbol{u}_h, w_h) = (f, w_h) \quad \forall\ w_h \in W_{h,0}^k, \tag{44}$$
$$(\boldsymbol{u}_{h,t}, \boldsymbol{v}_h) - (\sigma_h, \nabla \cdot \boldsymbol{v}_h) = 0 \qquad \forall\ \boldsymbol{v}_h \in \boldsymbol{V}_h^k, \tag{45}$$

with initial conditions

$$\sigma_h(\boldsymbol{x},0) = p_{1,I}(\boldsymbol{x}), \tag{46}$$
$$\boldsymbol{u}_{h,t}(\boldsymbol{x},0) = (\nabla p_0)_I(\boldsymbol{x}), \tag{47}$$

where, again, the finite element spaces $W_{h,0}^k$ and $\boldsymbol{V}_h^k$ are defined in (7)–(8) above. Note that $p_h(\boldsymbol{x},t) \in W_{h,0}^k$ can be recovered as

$$p_h(\boldsymbol{x},t) = \int_0^t \sigma_h(\boldsymbol{x},s)\,ds + p_{0,I}(\boldsymbol{x}). \tag{48}$$

Existence and uniqueness of a solution for (44)–(47) can be assured easily, since (44)–(45) can be rewritten as

$$A\sigma_t + BU = F, \tag{49}$$

$$DU_t - B^T\sigma = 0, \tag{50}$$

with A and D positive definite. So this is a system of (linear) ordinary differential equations, with the initial conditions (46)–(47), and a unique solution is known to exist.

The stability of (44)–(47) can be seen easily by choosing $w_h = \sigma_h$ and $\boldsymbol{v}_h = \boldsymbol{u}_h$ in (44) and (45) and adding the equations together. For the error analysis, we have the following result.

Theorem 4.1 *Assume $\sigma(\cdot,t) = p_t(\cdot,t)$, $\sigma_t(\cdot,t)$, $\boldsymbol{u}(\cdot,t) = -\nabla p(\cdot,t)$, $\boldsymbol{u}_t(\cdot,t)$ all lie in $H^{k+1}(\Omega)$. Let σ_h and $\boldsymbol{u}_h$ be the solution of (44)–(47) with mixed spaces (7)–(8), then the sub-optimal order error estimate*

$$||\sigma - \sigma_h||_{L^\infty(0,T;L^2(\Omega))} + ||\boldsymbol{u} - \boldsymbol{u}_h||_{L^\infty(0,T;L^2(\Omega))} \le Ch^k \tag{51}$$

holds, where $k \ge 1$ is the degree of the finite element spaces.

Proof. For any $\sigma_h \in W_{h,0}^k$ and $\boldsymbol{u}_h \in \boldsymbol{V}_h^k$, subtracting (44)–(45) from (42)–(43) yields

$$((\sigma_I - \sigma_h)_t, w_h) + (\nabla\cdot(\boldsymbol{u}_I - \boldsymbol{u}_h), w_h) = ((\sigma_I - \sigma)_t, w_h) + (\nabla\cdot(\boldsymbol{u}_I - \boldsymbol{u}), w_h), \tag{52}$$

$$((\boldsymbol{u}_I - \boldsymbol{u}_h)_t, \boldsymbol{v}_h) - (\sigma_I - \sigma_h, \nabla\cdot\boldsymbol{v}_h) = ((\boldsymbol{u}_I - \boldsymbol{u})_t, \boldsymbol{v}_h) - (\sigma_I - \sigma, \nabla\cdot\boldsymbol{v}_h). \tag{53}$$

Choosing $w_h = \sigma_I - \sigma_h \in W_{h,0}^k$ and $\boldsymbol{v}_h = \boldsymbol{u}_I - \boldsymbol{u}_h$ above, and adding the equations together, we obtain the following error estimate

$$\begin{aligned}
&\frac{1}{2}\frac{d}{dt}\big(||\sigma_I - \sigma_h||_0^2 + ||\boldsymbol{u}_I - \boldsymbol{u}_h||_0^2\big)\\
&\quad= ((\sigma_I - \sigma)_t, \sigma_I - \sigma_h) + (\nabla\cdot(\boldsymbol{u}_I - \boldsymbol{u}), \sigma_I - \sigma_h)\\
&\qquad+ ((\boldsymbol{u}_I - \boldsymbol{u})_t, \boldsymbol{u}_I - \boldsymbol{u}_h) - (\sigma_I - \sigma, \nabla\cdot(\boldsymbol{u}_I - \boldsymbol{u}_h))\\
&\quad\le Ch^{k+1}|\sigma_t|_{k+1}||\sigma_I - \sigma_h||_0 + Ch^k|\boldsymbol{u}|_{k+1}||\sigma_I - \sigma_h||_0\\
&\qquad+ Ch^{k+1}|\boldsymbol{u}_t|_{k+1}||\boldsymbol{u}_I - \boldsymbol{u}_h||_0 + Ch^{k+1}|\sigma|_{k+1}||\nabla\cdot(\boldsymbol{u}_I - \boldsymbol{u}_h)||_0.
\end{aligned}$$

Using the Cauchy-Schwarz inequality, the inverse estimate (10) and the Gronwall inequality, we have

$$||(\sigma_I - \sigma_h)(\cdot,t)||_0^2 + ||(\boldsymbol{u}_I - \boldsymbol{u}_h)(\cdot,t)||_0^2 \le Ch^{2k}.$$

Application of the triangle inequality and the interpolation estimate (9) concludes our proof. □

The discrete inf-sup conditions can be avoided for solving hyperbolic problems by mixed methods. The price we pay is that we only have sub-optimal order error estimates. When we choose the well-known mixed spaces satisfying the inf-sup condition, it is easy to show that optimal order error estimates can be achieved by a proof combining techniques given above and given for the for the elliptic problem using standard mixed spaces.

Remark 4.1 *Similar to the elliptic and parabolic problems, improved error estimates can be recovered on uniform grids by using Lin's integral identity (Lemma* 2.1*). For rectangular elements* $Q_k \times (Q_k)^d$ *or triangular* $P_1 \times (P_1)^d$*, using* (17) *and* (19) *above, we have the improved error estimate*

$$||\sigma - \sigma_h||_{L^\infty(0,T;L^2(\Omega))} + ||\boldsymbol{u} - \boldsymbol{u}_h||_{L^\infty(0,T;L^2(\Omega))} \leq Ch^{k+1/2}. \tag{54}$$

Remark 4.2 *Again, similar results hold true for fully time discrete approximations of* (44)–(47)*, provided that the time step is sufficiently small.*

5 Numerical Results

In this section we present numerical results on the problem (1)–(2) with $\Omega = (0,1)^2$. In our tests, we fix the true solution and define the corresponding function f accordingly.

5.1 Constant coefficient cases

Here let $\boldsymbol{g} = 0$ and $\alpha = \beta = 1$. The test cases are as follows:

Example 1, $p = x(1-x)y(1-y)\cos(xy)$;
Example 2, $p = y(1-y)(1+x)\sin(\pi x)$.

Table 1: Ex. 1 errors and convergence rates obtained on $Q_1 \times Q_1^2$ uniform grids

Variable	Mesh size	L^2 error	Convergence rate	L^∞ error	Convergence rate
Pressure	4×4	1.602E-3		6.066E-3	
	8×8	4.009E-4	2.00	1.803E-3	1.75
	16×16	1.005E-4	2.00	4.578E-4	1.98
	32×32	3.341E-5	1.59	1.147E-4	2.00
	64×64	1.197E-5	1.48	2.870E-5	2.00
Velocity	4×4	4.297E-3		1.226E-2	
	8×8	1.178E-3	1.87	3.925E-3	1.64
	16×16	2.994E-4	1.98	1.141E-3	1.78
	32×32	9.628E-5	1.64	3.052E-4	1.90
	64×64	3.549E-5	1.44	7.874E-5	1.96

We first solve these problems on various uniform meshes using continuous conforming $Q_1 \times Q_1^2$ rectangular elements and conforming $P_1 \times P_1^2$ triangular elements, for which $k = 1$. Detailed numerical results are presented in Tables 1–4, which show clearly the expected improved convergence rate $O(h^{3/2})$. In some cases, it appears that we see somewhat better results, up to a convergence of $O(h^2)$. In Figures 1–2, we show the computed pressure and velocity for Example 2 obtained on both uniform rectangles and uniform triangles. These results are consistent with our theoretical error analysis, and show that errors may converge even faster than we proved in some cases. Though a theoretical error analysis in the L^∞-norm is still open, we recorded these errors as well.

We then solved the problems on non-uniform rectangular and triangular meshes to see how well our mixed finite element spaces work. Detailed numerical results are presented in Tables 5–8, from

Table 2: Ex. 1 errors and convergence rates obtained on $P_1 \times P_1^2$ uniform grids

Variable	Mesh size	L^2 error	Convergence rate	L^∞ error	Convergence rate
Pressure	4×4	2.403E-3		8.867E-3	
	8×8	6.535E-4	1.88	2.291E-3	1.95
	16×16	1.728E-4	1.92	6.119E-4	1.90
	32×32	4.431E-5	1.96	1.644E-4	1.90
	64×64	1.115E-5	1.99	4.254E-5	1.95
Velocity	4×4	2.297E-2		1.009E-1	
	8×8	7.706E-3	1.58	5.902E-2	0.77
	16×16	2.247E-3	1.78	3.176E-2	0.89
	32×32	6.256E-4	1.84	1.642E-2	0.95
	64×64	1.653E-4	1.92	8.324E-3	0.98

Table 3: Ex. 2 errors and convergence rates obtained on $Q_1 \times Q_1^2$ uniform grids

Variable	Mesh size	L^2 error	Convergence rate	L^∞ error	Convergence rate
Pressure	4×4	8.738E-3		3.292E-2	
	8×8	2.197E-3	1.99	9.291E-3	1.83
	16×16	5.507E-4	2.00	2.330E-3	2.00
	32×32	1.378E-4	2.00	5.896E-4	1.98
	64×64	3.445E-5	2.00	1.476E-4	2.00
Velocity	4×4	3.787E-2		1.340E-1	
	8×8	8.917E-3	2.09	3.625E-2	1.89
	16×16	2.185E-3	2.03	1.013E-2	1.84
	32×32	5.413E-4	2.01	2.628E-3	1.95
	64×64	1.353E-4	2.00	6.660E-4	1.98

which we see clearly that $Q_1 \times Q_1^2$ and $P_1 \times P_1^2$ non-uniform rectangular meshes deliver at least the theoretically expected convergence of $O(h)$ in both the L^2- and L^∞-norms. The $P_1 \times P_1^2$ spaces consistently gave somewhat better results than the rectangular case. Moreover, in some cases the results are somewhat better than expected, but here never as good as $O(h^2)$. A selected numerical pressure and velocity for Example 2 obtained on nonuniform rectangles and triangles are shown in Figures 3–4.

Finally, we tested some unstructured triangular meshes generated using Delaunay triangulation. In many cases, we obtain even better results than on simple non-uniform triangle grids. One example is provided in Table 9, in which accuracy is better compared to Tables 8. In Figure 5 we show a selected numerical pressure and velocity for Example 2 obtained on unstructured triangular meshes.

The results of this section confirm computationally our view that our proposed simple mixed finite element spaces can be used effectively for solving a second order elliptic problem with a positive reaction term.

Table 4: Ex. 2 errors and convergence rates obtained on $P_1 \times P_1^2$ uniform grids

Variable	Mesh size	L^2 error	Convergence rate	L^∞ error	Convergence rate
Pressure	4×4	1.485E-2		5.583E-2	
	8×8	3.899E-3	1.93	1.434E-2	1.96
	16×16	1.021E-3	1.93	3.919E-3	1.87
	32×32	2.610E-4	1.97	1.066E-3	1.88
	64×64	6.570E-5	1.99	2.816E-4	1.92
Velocity	4×4	1.408E-1		0.6705	
	8×8	4.534E-2	1.63	0.3810	0.82
	16×16	1.301E-2	1.80	0.2022	0.91
	32×32	3.584E-3	1.86	0.1039	0.96
	64×64	9.275E-4	1.95	5.195E-2	1.00

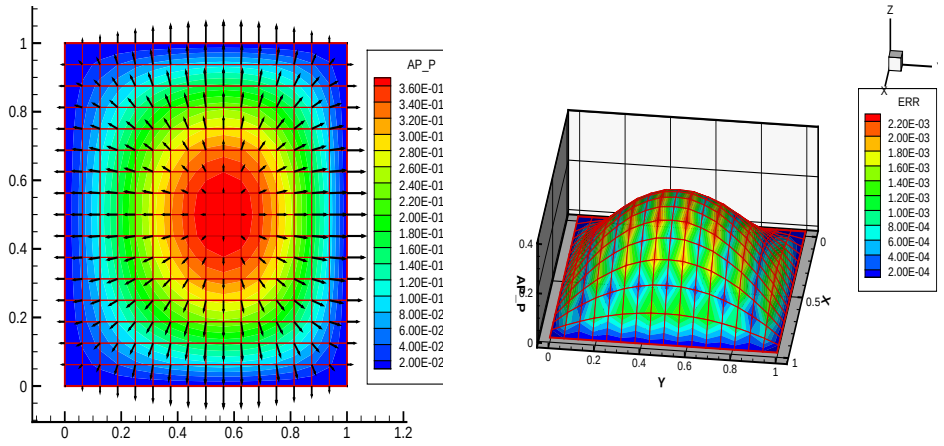

Figure 1: Ex. 2 results on a 16×16 uniform rectangular mesh. The left shows the computed pressure and velocity; the right shows the pointwise pressure error.

5.2 Variable coefficient case

Now let $\boldsymbol{g} = 0$, $\alpha = 1$, and $D = \mathrm{diag}(1 + xy, 1)$. We choose the exact solution as:

Example 3, $p = \sin(\pi x)\sin(2\pi y)$,

which is non-symmetric. The corresponding right hand side f is

$$f = (5 + xy)\pi^2 \sin(\pi x)\sin(2\pi y) - \pi y \cos(\pi x)\sin(2\pi y) + p.$$

We tested both $Q_1 \times (Q_1)^2$ and $P_1 \times (P_1)^2$ spaces on uniform rectangular mesh, uniform triangular mesh, non-uniform rectangular mesh, and non-uniform triangular mesh. The selected numerical results using Q_1 element are listed in Tables 10 - 11, which are consist with our theoretical analysis. The obtained numerical pressure and pointwise pressure error are shown in Fig. 6 and Fig. 7 for 64×64 uniform and nonuniform rectangular grids, respectively.

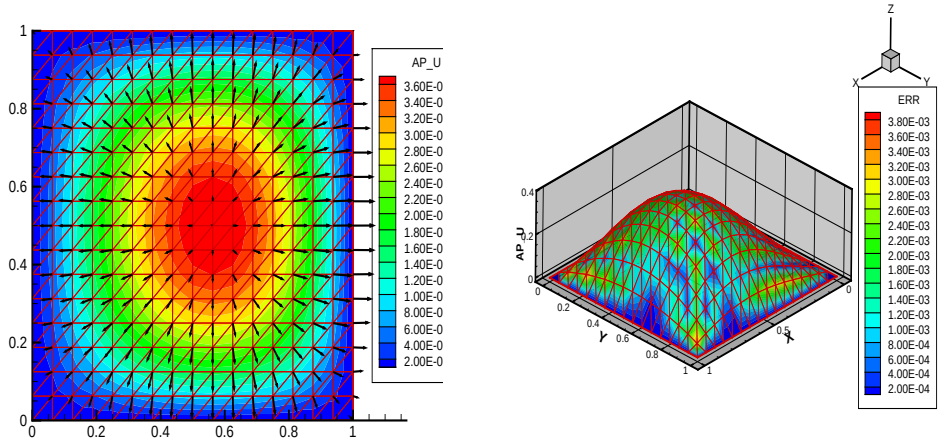

Figure 2: Ex. 2 results on a 16×16 uniform triangular mesh. The left shows the computed pressure and velocity; the right shows the pointwise pressure error.

Table 5: Ex. 1 errors and convergence rates obtained on $Q_1 \times Q_1^2$ nonuniform grids

Variable	Mesh size	L^2 error	Convergence rate	L^∞ error	Convergence rate
Pressure	4×4	2.363E-3		6.485E-3	
	8×8	5.047E-4	2.23	1.999E-3	1.70
	16×16	1.540E-4	1.71	9.529E-4	1.07
	32×32	6.951E-5	1.15	4.828E-4	0.98
	64×64	3.598E-5	0.95	2.386E-4	1.01
Velocity	4×4	3.357E-2		8.451E-2	
	8×8	1.547E-2	1.12	4.290E-2	0.98
	16×16	7.604E-3	1.02	2.050E-2	1.07
	32×32	3.794E-3	1.00	1.040E-2	0.98
	64×64	1.897E-3	1.00	5.319E-3	0.97

Table 6: Ex. 1 errors and convergence rates obtained on $P_1 \times P_1^2$ nonuniform grids

Variable	Mesh size	L^2 error	Convergence rate	L^∞ error	Convergence rate
Pressure	4×4	5.689E-3		1.381E-2	
	8×8	1.725E-3	1.72	5.678E-3	1.28
	16×16	5.484E-4	1.65	1.548E-3	1.87
	32×32	1.499E-4	1.87	4.135E-4	1.90
	64×64	3.879E-5	1.95	1.077E-4	1.94
Velocity	4×4	5.295E-2		1.847E-1	
	8×8	2.141E-2	1.31	1.218E-1	0.60
	16×16	7.630E-3	1.49	6.773E-2	0.85
	32×32	2.894E-3	1.40	3.568E-2	0.92
	64×64	1.096E-3	1.40	1.859E-2	0.94

Table 7: Ex. 2 errors and convergence rates obtained on $Q_1 \times Q_1^2$ nonuniform grids

Variable	Mesh size	L^2 error	Convergence rate	L^∞ error	Convergence rate
Pressure	4×4	1.572E-2		4.926E-2	
	8×8	5.179E-3	1.60	2.200E-2	1.16
	16×16	2.126E-3	1.28	9.589E-3	1.20
	32×32	9.819E-4	1.11	4.389E-3	1.13
	64×64	4.875E-4	1.01	2.114E-3	1.05
Velocity	4×4	2.124E-1		0.6403	
	8×8	9.329E-2	1.19	0.2410	1.41
	16×16	4.472E-2	1.06	0.1044	1.21
	32×32	2.206E-2	1.02	0.0518	1.01
	64×64	1.103E-2	1.00	2.571E-2	1.01

Table 8: Ex. 2 errors and convergence rates obtained on $P_1 \times P_1^2$ nonuniform grids

Variable	Mesh size	L^2 error	Convergence rate	L^∞ error	Convergence rate
Pressure	4×4	3.336E-2		9.044E-2	
	8×8	1.136E-2	1.55	3.593E-2	1.33
	16×16	3.422E-3	1.73	9.856E-3	1.87
	32×32	9.175E-4	1.90	2.667E-3	1.89
	64×64	2.374E-4	1.95	6.950E-4	1.94
Velocity	4×4	3.419E-1		0.7966	
	8×8	1.312E-1	1.38	0.4639	0.78
	16×16	4.667E-2	1.49	0.2339	0.99
	32×32	1.763E-2	1.40	0.1173	1.00
	64×64	6.680E-3	1.40	5.865E-2	1.00

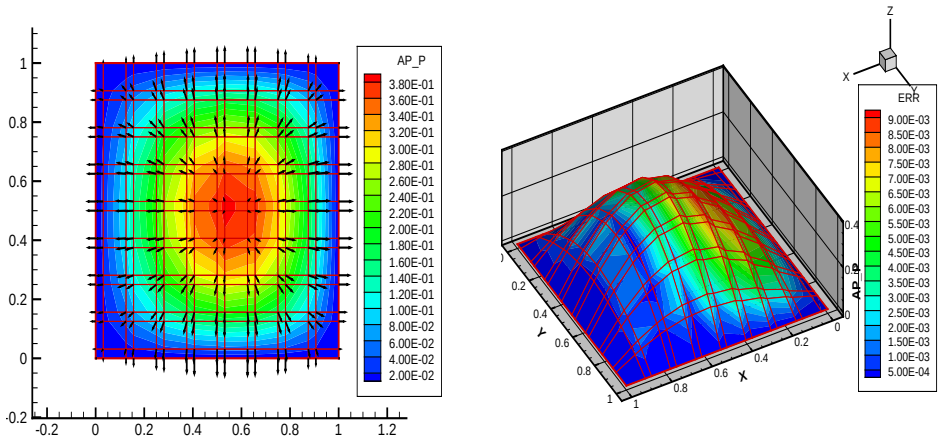

Figure 3: Ex. 2 results on a 16×16 nonuniform rectangular mesh. Left is the computed pressure and velocity. Right is the pointwise pressure error.

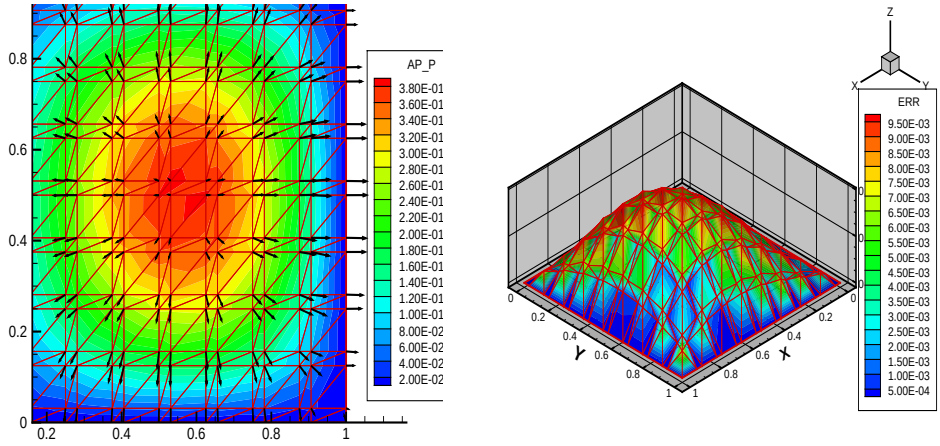

Figure 4: Ex. 2 results on a 16×16 nonuniform triangular mesh. Left is the computed pressure and velocity. Right is the pointwise pressure error.

Table 9: Ex. 2 errors and convergence rates obtained on $P_1 \times P_1^2$ unstructured triangles

Variable	Number of nodes	Number of elements	L^2 error	Convergence rate	L^∞ error	Convergence rate
Pressure	13	16	1.227E-2		6.398E-2	
	33	48	7.168E-3	0.78	2.658E-2	1.27
	123	212	1.676E-3	2.10	7.614E-3	1.80
	469	872	5.160E-4	1.70	2.684E-3	1.50
	1807	3484	1.834E-4	1.49	6.157E-4	2.12
Velocity	13	16	2.215E-1		4.850E-1	
	33	48	3.930E-2	2.50	1.093E-1	2.15
	123	212	1.474E-2	1.41	4.791E-2	1.19
	469	872	6.390E-3	1.21	3.117E-2	0.62
	1807	3484	4.120E-3	0.63	1.892E-2	0.72

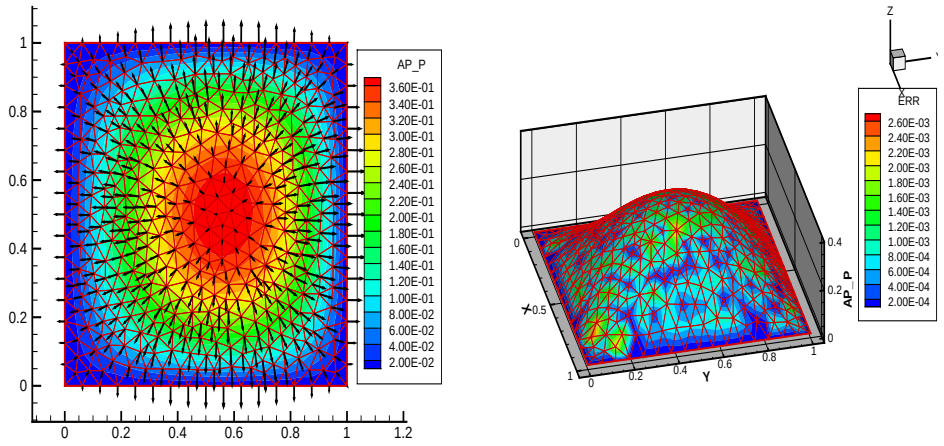

Figure 5: Ex. 2 results on 872 unstructured triangles. The left shows the computed pressure and velocity; the right shows the pointwise pressure error.

Table 10: Ex. 3 errors and convergence rates obtained on $Q_1 \times Q_1^2$ uniform grids

Variable	Mesh size	L^2 error	Convergence rate	L^∞ error	Convergence rate
Pressure	4×4	4.1232E-2		0.1668	
	8×8	8.5088E-3	2.276	3.4578E-2	2.270
	16×16	2.0429E-3	2.058	8.3090E-3	2.057
	32×32	5.0584E-4	2.013	2.0554E-3	2.015
	64×64	1.2646E-4	2.000	5.1345E-4	2.001
Velocity	4×4	0.2420		0.7352	
	8×8	6.0794E-2	1.993	0.2025	1.860
	16×16	1.5165E-2	2.003	5.1154E-2	1.985
	32×32	3.7873E-3	2.001	1.2813E-2	1.997
	64×64	9.4683E-4	2.000	3.2042E-3	1.999

Table 11: Ex. 3 errors and convergence rates obtained on $Q_1 \times Q_1^2$ non-uniform grids

Variable	Mesh size	L^2 error	Convergence rate	L^∞ error	Convergence rate
Pressure	4×4	0.2036		1.0570	
	8×8	6.5093E-2	1.645	0.3133	1.754
	16×16	2.9069E-2	1.163	0.1358	1.206
	32×32	1.4131E-2	1.040	6.5834E-2	1.044
	64×64	7.0167E-2	1.010	3.2667E-2	1.011
Velocity	4×4	1.1083		1.7814	
	8×8	0.3518	1.655	0.7902	1.172
	16×16	0.1575	1.159	0.2917	1.437
	32×32	7.6191E-2	1.047	0.1244	1.229
	64×64	3.8095E-2	1.000	6.0801E-2	1.032

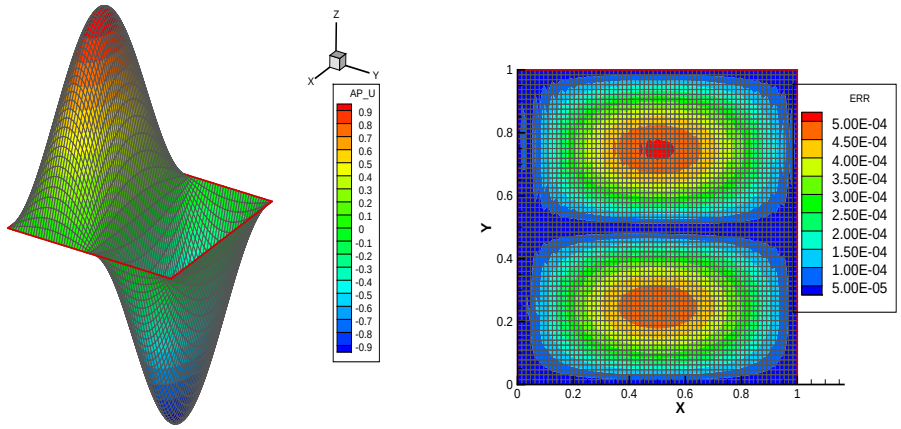

Figure 6: Ex. 3 results on a 64×64 uniform rectangular mesh. Left is the computed pressure. Right is the pointwise pressure error.

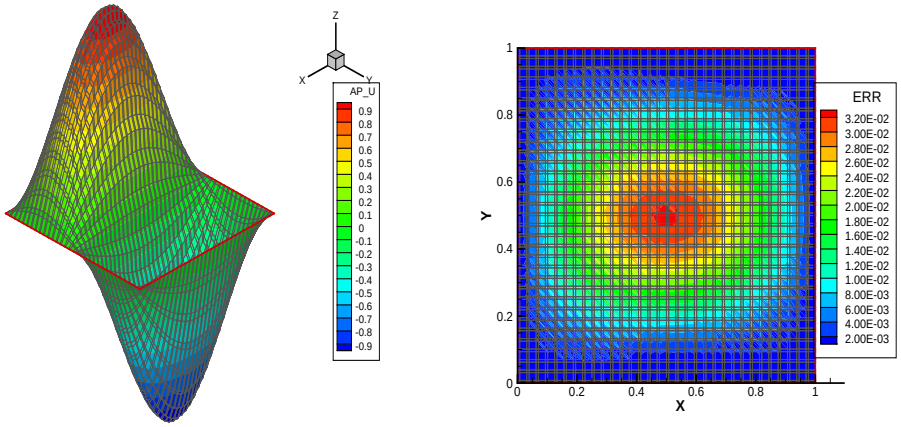

Figure 7: Ex. 3 results on a 64×64 nonuniform rectangular mesh. Left is the computed pressure. Right is the pointwise pressure error.

5.3 Comparison with the lowest-order Raviart-Thomas element

In this section, we present a numerical comparison of our proposed method with the traditional mixed method using the lowest-order Raviart-Thomas triangular element (i.e., the RT_0 element). Our implementation of RT_0 is modified from the Matlab program EBmfem [4] by adding a lower-order reaction term to the model equation. We solved Example 2 using both our method and the RT_0 triangular element, and compared the maximum error of p at the barycenter of each element. As for numerical efficiency, we compare the condition numbers of the resulting matrices from both methods (i.e., we use the **cond** Matlab command), since the condition number dominates the solution time, independent of the implementation.

The results obtained on uniform and unstructured triangular grids are presented in Tables 12 and 13, respectively. From our results, it is interesting to note three things. First, the RT_0 method is a little more accurate compared to our $P_1 \times P_1^2$ method. More specifically, on uniform meshes, the L^∞ error from our method is about three times larger than that obtained by the RT_0 method for the same grid; while on unstructured meshes, the error from our method is only about one to two times larger than that obtained by the RT_0 method. Second, our results show that the maximum errors at the barycenters of the elements on both uniform and unstructured meshes are convergent to order $O(h^2)$, with the exception of the last RT_0 unstructured mesh, which we attribute to the ill-condition of the system. Note that $O(h^2)$ is better than what we could prove for the $P_1 \times P_1^2$ method, and $O(h^2)$ for the RT_0 method was proved in [16, Corollary 6.2]. Finally, we see that the condition numbers of our method are a little better than the RT_0 method on uniform meshes, and significantly so on unstructured meshes. This implies that our method will be more efficient in its solution time when an iterative solver is used, and less subject to rounding error when a direct solver is used.

Table 12: Comparison of p between $P_1 \times P_1^2$ and RT_0 on uniform triangular grids

	L^∞ error at the barycenter		Condition number	
Mesh size	$P_1 \times P_1^2$ method	RT_0 method	$P_1 \times P_1^2$ method	RT_0 method
4×4	3.7894E-2	8.8204E-3	72.68	71.14
8×8	1.0206E-2	2.8443E-3	158.37	198.52
16×16	2.6405E-3	7.8486E-4	326.84	465.93
32×32	6.7103E-4	2.0904E-4	659.69	1073.19

Table 13: Comparison of p between $P_1 \times P_1^2$ and RT_0 on unstructured triangular grids

	L^∞ error at the barycenter		Condition number	
Number of elements	$P_1 \times P_1^2$ method	RT_0 method	$P_1 \times P_1^2$ method	RT_0 method
48	1.6892E-2	6.8893E-3	44.16	139.97
212	3.9573E-3	1.7953E-3	90.45	337.01
872	1.0476E-3	1.0483E-3	257.26	786.95

6 Conclusions

In this paper, we investigated the mixed finite element method for a second order elliptic problem with a uniformly positive zeroth order term (e.g., single phase flow in porous media with a reaction term), and found that specially designed mixed finite element spaces satisfying the inf-sup condition are not needed. Instead, in d dimensions, we can use the standard nodal-based finite element spaces $Q_k \times (Q_k)^d$ on rectangles or $P_k \times (P_k)^d$ on simplices to solve for both the scalar (e.g., pressure) and flux (e.g., velocity) field. The price we pay for violating the inf-sup condition is that we only have sub-optimal order error estimates, losing a single power of the mesh parameter h in the estimate. Moreover, the bounding constant degenerates as the infimum of the lowest order term tends to zero.

We also noted a locally conservative variant, defined simply by approximating the scalar variable in a discontinuous space of piecewise polynomials. On simplicial meshes, the continuous spaces for all $k \geq 1$ and the discontinuous spaces for $k > 1$ have fewer degrees of freedom than the Raviart-Thomas spaces giving similar accuracy. On rectangular meshes, these proposed spaces are slightly larger than the Raviart-Thomas spaces, however the former are much simpler to implement, especially when higher order spaces are desired, or when an *hp*-adaptive refinement procedure is implemented.

With a delicate superconvergence analysis, we found that we could improve the error estimates by one-half power of h provided the solution has one extra order of regularity and we use either $Q_k \times (Q_k)^d$ on a uniform rectangular grid or $P_1 \times (P_1)^d$ on a uniform simplicial mesh. Moreover, we recover a full power of h when the problem has periodic boundary conditions.

We extended our results to time-dependent parabolic and hyperbolic problems. These problems do not require a positive zeroth order term. For sufficiently small time steps, the Gronwall inequality enables us to prove that standard nodal-based finite element spaces give results similar to the elliptic case.

Finally, numerical results supporting our analysis were presented using the most popular spaces $Q_1 \times (Q_1)^2$ and $P_1 \times (P_1)^2$. Although much simpler to use, the rectangular elements use exactly three more degrees of freedom as the Raviart-Thomas spaces. Moreover, mainly because the scalar space is continuous, our triangular and tetrahedral element spaces have many fewer degrees of freedom than the Raviart-Thomas spaces, and are more easily implemented, especially in an *hp*-adaptive procedure. At least in some cases, our method produces linear systems that have smaller condition numbers than corresponding standard RT_0 spaces.

In certain cases, the standard spaces are competitive with, and perhaps superior to, standard mixed spaces satisfying the inf-sup condition. Because of their simplicity and convergence properties, the standard spaces are especially attractive when (1) simplicial meshes are used, (2) problems with periodic boundary conditions (such as cell problems in homogenization) are approximated with uniform rectangular grids, (3) higher order approximations are desired, and (4) when an *hp*-adaptive refinement procedure is implemented.

Acknowledgment

The authors thank an anonymous referee for his/her insightful comments that improved the paper.

7 Appendix

In this appendix, we provide a proof of Lemma 2.1 in the case of $k = 1$ for Q_1 elements.

Proof of (17) *for* Q_1 *elements.* We assume for simplicity of exposition that $\Omega \subset \boldsymbol{R}^2$. Take a typical rectangular element $\tau \in T_h$ with center at (x_τ, y_τ) and lengths $2h_\tau$ and $2k_\tau$ in the x- and y-directions, respectively. Note that for any $v \in Q_1(\tau)$, we can expand it as

$$v(x,y) = v(x_\tau, y_\tau) + (x - x_\tau)v_x(y_\tau) + (y - y_\tau)v_y(x_\tau) + (x - x_\tau)(y - y_\tau)v_{xy},$$

from which we see that evaluation of $\int_\tau (w - w_I)_x \, v \, dx \, dy$ requires evaluating the four terms

$$\int_\tau (w - w_I)_x \, dx \, dy, \qquad \int_\tau (w - w_I)_x (x - x_\tau) \, dx \, dy,$$
$$\int_\tau (w - w_I)_x (y - y_\tau) \, dx \, dy, \quad \int_\tau (w - w_I)_x (x - x_\tau)(y - y_\tau) \, dx \, dy.$$

We need two special functions:

$$E(x) = \frac{1}{2}((x - x_\tau)^2 - h_\tau^2) \quad \text{and} \quad F(y) = \frac{1}{2}((y - y_\tau)^2 - k_\tau^2).$$

Using the fact that $F''(y) = 1$ and integration by parts, we have

$$\begin{aligned}
\int_\tau (w - w_I)_x \, dx \, dy &= \int_\tau (w - w_I)_x F''(y) \, dy \, dx \\
&= \int_{x_\tau - h_\tau}^{x_\tau + h_\tau} (w - w_I)_x F'(y) \Big|_{y = y_\tau - k_\tau}^{y_\tau + k_\tau} dx - \int_\tau (w - w_I)_{xy} F'(y) \, dx \, dy \\
&= \int_\tau (w - w_I)_{xyy} F(y) \, dx \, dy = \int_\tau w_{xyy} F(y) \, dx \, dy,
\end{aligned}$$

where in the above we used the facts that $w - w_I = 0$ at the vertices of τ, $F(y) = 0$ at edges $y = y_\tau \pm k_\tau$, and $w_{I,yy} = 0$.

Using the identity $x - x_\tau = E'(x)$ and integration by parts, we obtain

$$\begin{aligned}
\int_\tau (w - w_I)_x (x - x_\tau) \, dx \, dy &= \int_\tau (w - w_I)_x E'(x) \, dx \, dy \\
&= \int_{y_\tau - k_\tau}^{y_\tau + h_\tau} (w - w_I)_x E(x) \Big|_{x = x_\tau - h_\tau}^{x_\tau + h_\tau} dy - \int_\tau (w - w_I)_{xx} E(x) \, dx \, dy \\
&= - \int_\tau w_{xx} E(x) \, dx \, dy, \qquad (55)
\end{aligned}$$

where we used the facts that $E(x) = 0$ at edges $x = x_\tau \pm h_\tau$, and $w_{I,xx} = 0$. Furthermore, using the identity $E(x) = \frac{1}{6}(E^2(x))'' - \frac{1}{3}h_\tau^2$ in (55) and integrating by parts, we have

$$\begin{aligned}
\int_\tau (w - w_I)_x (x - x_\tau) \, dx \, dy &= - \int_\tau w_{xx} \left[\frac{1}{6}(E^2(x))'' - \frac{1}{3}h_\tau^2 \right] dx \, dy \\
&= \int_\tau w_{xxx} \frac{1}{6}(E^2(x))' \, dx \, dy + \frac{1}{3}h_\tau^2 \int_\tau w_{xx} \, dx \, dy \\
&= \frac{1}{3} \int_\tau w_{xxx} E(x) \, (x - x_\tau) \, dx \, dy + \frac{1}{3}h_\tau^2 \int_\tau w_{xx} \, dx \, dy,
\end{aligned}$$

wherein we used that $(E^2(x))' = 0$ and $E(x) = 0$ at edges $x = x_\tau \pm h_\tau$.

Using the identity $y - y_\tau = \frac{1}{6}(F^2(y))'''$, we have

$$\begin{aligned}\int_\tau (w - w_I)_x (y - y_\tau)\,dx\,dy &= \int_\tau (w - w_I)_x \frac{1}{6}(F^2(y))'''\,dx\,dy \\ &= -\int_\tau (w - w_I)_{xy} \frac{1}{6}(F^2(y))''\,dx\,dy \\ &= \int_\tau (w - w_I)_{xyy} \frac{1}{6}(F^2(y))'\,dx\,dy \\ &= \int_\tau w_{xyy} \frac{1}{6}(F^2(y))'\,dx\,dy = \int_\tau w_{xyy} \frac{1}{3}F(y)(y - y_\tau)\,dx\,dy,\end{aligned}$$

where we used the facts that $w - w_I = 0$ at the vertices of τ, $(F^2(y))' = 0$ at edges $y = y_\tau \pm k_\tau$, and $w_{I,yy} = 0$.

Finally, using the identities $x - x_\tau = E'(x)$ and $y - y_\tau = F'(y)$, we obtain

$$\begin{aligned}\int_\tau (w - w_I)_x (x - x_\tau)(y - y_\tau)\,dx\,dy &= \int_\tau (w - w_I)_x E'(x)F'(y)\,dx\,dy \\ &= -\int_\tau (w - w_I)_{xx} E(x)F'(y)\,dx\,dy \\ &= \int_\tau w_{xxy} E(x)F(y)\,dx\,dy,\end{aligned}$$

where we used the facts that $E(x) = 0$ at edges $x = x_\tau \pm h_\tau$ and $F(y) = 0$ at edges $y = y_\tau \pm k_\tau$.

Combining the above four estimates yields

$$\begin{aligned}\int_\tau (w - w_I)_x\, v\,dx\,dy = &\int_\tau w_{xyy} F(y)\, v(x_\tau, y_\tau)\,dx\,dy + \frac{1}{3}\int_\tau w_{xxx} E(x)(x - x_\tau) v_x(y_\tau)\,dx\,dy \\ &+ \frac{1}{3}h_\tau^2 \int_\tau w_{xx} v_x(y_\tau)\,dx\,dy + \frac{1}{3}\int_\tau w_{xyy} F(y)(y - y_\tau) v_y(x_\tau)\,dx\,dy \\ &+ \int_\tau w_{xxy} E(x)F(y) v_{xy}\,dx\,dy. \qquad (56)\end{aligned}$$

Expanding the functions v, v_x, v_y, and v_{xy} in terms of general point (x, y), as in

$$v(x_\tau, y_\tau) = v(x, y) + (x_\tau - x)v_x(y) + (y_\tau - y)v_y(x) + (x_\tau - x)(y_\tau - y)v_{xy},$$

noting that E is $O(h_\tau^2) = O(h^2)$, F is $O(k_\tau^2) = O(h^2)$, $x - x_\tau$ and $y - y_\tau$ are $O(h)$, and using the Cauchy-Schwarz inequality and the inverse estimate (10), we see that

$$\int_\tau (w - w_I)_x\, v\,dx\,dy = O(h^2)||w||_{3,\tau}||v||_{0,\tau} + \frac{1}{3}h_\tau^2 \int_\tau w_{xx} v_x(y_\tau)\,dx\,dy. \qquad (57)$$

But integration by parts gives us

$$\begin{aligned}&\frac{1}{3}h_\tau^2 \int_\tau w_{xx} v_x(y_\tau)\,dx\,dy \\ &\quad = \frac{1}{3}h_\tau^2 \int_\tau w_{xx}[v_x(y) + F'(y)v_{xy}]\,dx\,dy \\ &\quad = \frac{1}{3}h_\tau^2 \int_{y_\tau - k_\tau}^{y_\tau + k_\tau} w_{xx} v \Big|_{x = x_\tau - h_\tau}^{x_\tau + h_\tau} dy - \frac{1}{3}h_\tau^2 \int_\tau w_{xxx} v\,dx\,dy - \frac{1}{3}h_\tau^2 \int_\tau w_{xxy} F(y) v_{xy}\,dx\,dy, \qquad (58)\end{aligned}$$

where we used the fact that $F(y) = 0$ at edges $y = y_\tau \pm k_\tau$.

Hence if $v \in W^1_{h,0}$ and the grid is uniform ($h_\tau = h$ and $k_\tau = k$ for all τ), summing up all the element edges will eliminate the boundary integral in (58), which combining with (57) yields

$$|((w - w_I)_x, v)| \le Ch^2 ||w||_3 ||v||_0. \tag{59}$$

Results for the other Cartesian directions are obtained by symmetry.

Finally, we note that we could have optimal error estimates for some special cases. The final statement in Lemma 2.1 is the case where w is periodic (actually, we only need that w_{xx} is periodic in x and w_{yy} is periodic in y). The boundary integral in (58) will vanish for any $v_h \in W^k_h$, and we recover the optimal error estimate. □

References

[1] T. Arbogast and Ch.-S. Huang, A fully mass and volume conserving implementation of a characteristic method for transport problems, SIAM J. Sci. Comput. 28 (2006) 2001–2022.

[2] T. Arbogast, M.F. Wheeler and I. Yotov, Mixed finite elements for elliptic problems with tensor coefficients as cell-centered finite differences, SIAM J. Numer. Anal. 34 (1997) 828–852.

[3] T. Arbogast and M.F. Wheeler, A family of rectangular mixed elements with a continuous flux for second order elliptic problems, SIAM J. Numer. Anal. 42 (2005) 1914–1931.

[4] C. Bahriawati and C. Carstensen, Three MATLAB implementations of the lowest-order Raviart-Thomas MFEM with a posteriori error control, Comput. Methods Appl. Math. 5 (2005) 333–361.

[5] F. Brezzi, J. Douglas, Jr., and L.D. Marini, Two families of mixed finite elements for second order elliptic problems, Numer. Math. 47 (1985) 217–235.

[6] F. Brezzi, J. Douglas, Jr., R. Duràn and M. Fortin, Mixed finite elements for second order elliptic problems in three variables, Numer. Math. 51 (1987) 237–250.

[7] F. Brezzi and M. Fortin, Mixed and Hybrid Finite Element Methods, Springer-Verlag, New York, 1991.

[8] F. Brezzi, M. Fortin and L.D. Marini, Mixed finite element methods with continuous stresses, Math. Models and Meth. in Appl. Sci. 3 (1993) 275–287.

[9] C.M. Chen and Y.Q. Huang, High Accuracy Theory of Finite Element Methods (in Chinese), Hunan Science Press, China, 1995.

[10] H. Chen, R. Ewing and R. Lazarov, Superconvergence of mixed finite element methods for parabolic problems with nonsmooth initial data, Numer. Math. 78 (1998) 495–521.

[11] Y.P. Chen and Y.Q. Huang, Improved error estimates for mixed finite element for nonlinear hyperbolic equations: the continuous-time case, J. Comput. Math. 19 (2001) 385–392.

[12] Z. Chen and J. Douglas, Jr., Prismatic mixed finite elements for second order elliptic problems, Calcolo 26 (1989) 135–148.

[13] L. Cowsar, T.F. Dupont and M.F. Wheeler, A priori estimates for mixed finite element approximations of second-order hyperbolic equations with absorbing boundary conditions, SIAM J. Numer. Anal. 33 (1996) 492–504.

[14] J. Douglas, Jr., R.E. Ewing, and M.F. Wheeler, Approximation of the pressure by a mixed method in the simulation of miscible displacement, R.A.I.R.O. Modél. Math. Anal. Numér., 17 (1983) 17–33.

[15] A. Friedman, Partial Differential Equations of Parabolic Type, Prentice-Hall, Englewood Cliffs, New Jersey, 1964.

[16] L. Gastaldi and R. Nochetto, Optimal L^∞-error estimates for nonconforming and mixed finite element methods of lowest order, Numer. Math. 50 (1987) 587–611.

[17] T.J.R. Hughes, L.P. Franca and M. Balestra, A new finite element formulation for computational fluid dynamics. V. Circumventing the Babuska-Brezzi condition: a stable Petrov-Galerkin formulation of the Stokes problem accommodating equal-order interpolations, Comput. Methods Appl. Mech. Engrg. 59 (1986) 85–99.

[18] E.W. Jenkins, B. Riviére and M.F. Wheeler, A priori error estimates for mixed finite element approximations of the acoustic wave equation, SIAM J. Numer. Anal. 40 (2002) 1698–1715.

[19] C. Johnson and V. Thomée, Error estimates for some mixed finite element methods for parabolic type problems, RAIRO Anal. Numer. 15 (1981) 41–78.

[20] Q. Lin, A rectangle test for finite element analysis, Prof. of Sys. Sci. & Sys. Engrg., Great Wall (H.K.) Culture Publish Co., 1991, pp. 213–216.

[21] Q. Lin, J. Li and A. Zhou, A rectangle test for the Stokes equations, Prof. of Sys. Sci. & Sys. Engrg., Great Wall (H.K.) Culture Publish Co., 1991, pp. 240–241.

[22] Q. Lin and N. Yan, The Construction and Analysis of High Accurate Finite Element Methods (in Chinese), Hebei University Press, Hebei, China, 1996.

[23] Q. Lin, N. Yan and A. Zhou, A rectangle test for interpolated finite elements, Prof. of Sys. Sci. & Sys. Engrg., Great Wall (H.K.) Culture Publish Co., 1991, pp. 217–229.

[24] J.-C. Nédélec, Mixed finite elements in R^3, Numer. Math. 35 (1980) 315–341.

[25] J.T. Oden and G.F. Carey, Finite Elements: Mathematical Aspects, Vol.IV, Prentice Hall, Englewood Cliffs, NJ, 1983.

[26] R.A. Raviart and J.M. Thomas, A mixed finite element method for 2nd order elliptic problems, in Mathematical Aspects of Finite Element Methods, I. Galligani and E. Magenes, eds., Lecture Notes in Math. 606, Springer-Verlag, New York, 1997, pp. 292–315.

[27] J. E. Roberts and J.M. Thomas, Mixed and Hybrid Methods, Handbook of Numerical Analysis, Vol. 2, Finite Element Methods (Part 1), P. G. Ciarlet and J. L. Lions (eds.), Elsevier Science Publishers B.V. (North-Holland), Amsterdam, 1991, pp. 523–639.

[28] T.F. Russell and M.F. Wheeler, Finite element and finite difference methods for continuous flows in porous media, in The Mathematics of Reservoir Simulation, R. E. Ewing, ed., Frontiers in Applied Mathematics, n. 1, Society for Industrial and Applied Mathematics, Philadelphia, 1983, pp. 35–106 (Chapter II).

[29] T.E. Tezduyar, S. Mittal, S.E. Ray and R. Shih, Incompressible flow computations with stabilized bilinear and linear equal-order-interpolation velocity-pressure elements, Comput. Methods Appl. Mech. Engrg. 95 (1992) 221–242.

[30] Y.D. Wang, The L^2 Theory of Partial Differential Equations (in Chinese), Beijing University Press, Beijing, 1989.

[31] A. Weiser and M.F. Wheeler, On convergence of block-centered finite-differences for elliptic

problems, SIAM J. Numer. Anal. 25 (1988) 351–375.

[32] A. Zhou, An analysis of some high accuracy finite element methods for hyperbolic problems, SIAM J. Numer. Anal. 39 (2001) 1014–1028.

[33] A. Zhou and J. Li, The full approximation accuracy for the stream function-vorticity-pressure method, Numer. Math. 68 (1994) 427–435.